Ultrasonic Measurement of Change in Elasticity due to Endothelium Dependent Relaxation Response by Accurate Detection of Artery-Wall Boundary

Takuya KANEKO, Hideyuki HASEGAWA, and Hiroshi KANAI*

Graduate School of Engineering, Tohoku University, Sendai 980-8579, Japan

Ross hypothesized that an endothelial dysfunction is considered to be an initial step in atherosclerosis. Endothelial cells, which release nitric oxide (NO) in response to shear stress from blood flow, have a function of relaxing smooth muscle in the media of the arterial wall. For the assessment of the endothelial function, there is a conventional method in which the change in the diameter of the brachial artery caused by flow-mediated dilation (FMD) is measured with ultrasound. However, despite the fact that the collagen-rich hard adventitia does not respond to NO, the conventional method measures the change in diameter depending on the mechanical property of the entire wall including the adventitia. Therefore, we developed a method of measuring the change in the thickness and the elasticity of the brachial artery during a cardiac cycle using the *phased tracking method* for the evaluation of the mechanical property of only the intima-media region. In this study, the initial positions of echoes from the lumen-intima and media-adventitia boundaries are determined using complex template matching to accurately estimate the minute change in the thickness and the elasticity of the brachial and radial arteries. The ambiguity in the determination of such boundaries was eliminated using complex template matching, and the change in elasticity measured by the proposed method was larger than the change in inner diameter obtained by the conventional method.
[DOI: 10.1143/JJAP.46.4881]

KEYWORDS: complex template matching, elasticity, atherosclerosis, endothelial dysfunction, nitric oxide, flow-mediated dilation

1. Introduction

The main cause of circulatory diseases is considered to be atherosclerosis. Ross hypothesized that endothelial dysfunction is considered to be the initial step in atherosclerosis.[1] Consequently, it is important to diagnose the endothelial dysfunction for early preventive treatment.

Morphologically, the arterial wall consists of three concentric layers called intima, media, and adventitia.[2] In normal muscular arteries, the tunica intima consists of mono-layered endothelial cells. The media is composed predominantly of smooth muscle cells. The adventitia, which is composed of fibrous connective tissue, covers the outside of the intima-media complex. Endothelial cells mainly adjust the distensibility of blood vessels and maintain vascular homeostasis.

Although there are techniques for evaluating the intima-media thickness[3,4] and elasticity of an arterial wall[5–7] for the diagnosis of atherosclerosis, flow-mediated dilation (FMD) measurements in brachial and other conduit arteries have become popular means of evaluating the endothelial function for the early diagnosis of atherosclerosis.[8,9] Endothelial cells, which release nitric oxide (NO) in response to shear stress from blood flow,[10] have a function of relaxing smooth muscle in the media of the arterial wall. In FMD measurement, the endothelium-dependent change in inner diameter in response to reactive hyperemia is measured by comparing the luminal diameter of the brachial artery before and after the ischemia of the forearm induced by pressurizing a cuff. However, the collagen-rich hard adventitia does not respond to NO. Therefore, the conventional method underestimates the FMD caused by an endothelial response because the change in inner diameter depends on not only the mechanical properties of the intima and media but also that of the adventitia.

Sugimoto *et al.* proposed a method of measuring the change in thickness and the elasticity of the brachial arterial wall during a heart cycle using the *phased tracking method* to evaluate the change in the mechanical property of only the intima-media region.[11–13] In this measurement, a method is necessary to assign the boundaries of the intima-media layer for objective assessment. If a conventional edge detector such as the simple thresholding of magnitude is applied to the ultrasonic RF signal, many fragmented edges in the arterial wall will be detected by the influences of scatterers and interfaces, and the true media-adventitia boundary is not easily identified because an echo from the media-adventitia boundary includes redundant echoes from the intima-media complex. Fun *et al.* proposed a technique for the boundary detection of the brachial arterial wall using the template matching between an envelope of the ultrasonic RF signal and an adaptive approximate Gaussian model.[14]

In this study, the lumen-intima boundary (LIB) and media-adventitia boundary (MAB) are detected using the complex template matching between the measured complex demodulated signal and the adaptive complex model signal to obtain transients in the change in thickness and the elasticity of the intima-media region. Additionally, the proposed method is applied to the measurement of conventional FMD, the change in intima-media thickness, and the elasticity of the radial artery using high-frequency ultrasound. FMD measurement in the radial artery, particularly the measurements of the change in elasticity due to an endothelium-dependent relaxation response, has not yet been reported in the literature. There is an inversely proportional relation between FMD value and the inner diameter of the artery at rest because flow rate, which is related to shear stress, is inversely proportional to the inner diameter.[15] Therefore, the radial artery would be a more suitable site for the measurement of FMD.

2. Principles

2.1 Elastic modulus estimation of arterial wall

To calculate a minute change in wall thickness caused by

---

*E-mail address: hkanai@ecei.tohoku.ac.jp

a heartbeat, the velocity of the artery-wall boundary is estimated.[11] The velocity $v(t)$ is estimated from the phase shift $\Delta\theta(t)$ of echoes in two consecutive frames. The phase shift $\Delta\theta(t)$ is obtained on the basis of the cross-correlation applied to the demodulated signal $z(t; d + x(t))$ of RF echo reflected at a depth $d + x(t)$ at a time t, where d and $x(t)$ are the initial depth set at $t = 0$ and the displacement of the arterial wall in the direction of depth, respectively. From the estimated phase shift $\Delta\hat{\theta}(t)$, the velocity of the arterial wall during a pulse repetition interval ΔT is obtained as

$$\hat{v}(t) = -\frac{c_0}{2\omega_0}\frac{\Delta\hat{\theta}(t)}{\Delta T}, \qquad (2.1)$$

where ω_0 and c_0 are the center angular frequency of the ultrasound wave and the speed of sound, respectively. The change in thickness, $\Delta h(t)$, between two different positions in the arterial wall along an ultrasonic beam is obtained from the difference between displacements, $x_A(t)$ and $x_B(t)$, at these two positions as

$$\Delta\hat{h}(t) = \hat{x}_A(t) - \hat{x}_B(t)$$
$$= \int_0^t \{\hat{v}_A(t) - \hat{v}_B(t)\}\,\mathrm{d}t. \qquad (2.2)$$

The change in thickness, $\Delta h(t)$, corresponds to the incremental strain in the radial direction at a time t due to a pressure increment, $\Delta p(t)$, from the diastolic pressure. Therefore, from the maximum change in wall thickness, $\Delta h_{max} = \max|\Delta h(t)|$, and the pulse pressure $\Delta p_{max} = \max \Delta p(t)$, which is the difference between the systolic and diastolic pressures, the approximate circumferential elastic modulus E_θ^h is obtained as[12]

$$E_\theta^h \approx \frac{1}{2}\left(\frac{r_0}{h_0} + 1\right)\frac{\Delta p_{max}}{\dfrac{\Delta h_{max}}{h_0}}, \qquad (2.3)$$

where r_0 and h_0 are the internal diameter and wall thickness at the end diastole, respectively.

2.2 Determination of optimum initial positions of artery-wall boundaries

Figure 1 shows the cross-sectional ultrasonic images of the brachial and radial arteries. As shown in Fig. 1, along an ultrasonic beam, the ultrasonic echo reflected from the LIB of the posterior wall can be found, the amplitude of the echo slightly decreases in the media region, and it increases again around the MAB.[16] In this study, echoes from LIB and MAB of the posterior wall should be tracked to accurately obtain the minute change in the intima-media thickness and elasticity. However, it is difficult to detect the MAB of the arterial wall because weak echoes from the intima-media region overlap with the echo from the MAB, and the leading edge of the echo from the MAB is not clear. Therefore, the MAB cannot be determined directly from the B-mode image shown in Fig. 1. Consequently, in this study, a method of detecting the initial positions of these boundaries using the complex template matching between RF echoes and model echoes is investigated, and is applied to the detection of the LIB and MAB of the posterior wall.

Figure 2 shows a schematic view of ultrasonic echoes from the artery-wall boundaries. The ultrasonic echo signal from the posterior wall includes mainly echoes from the LIB
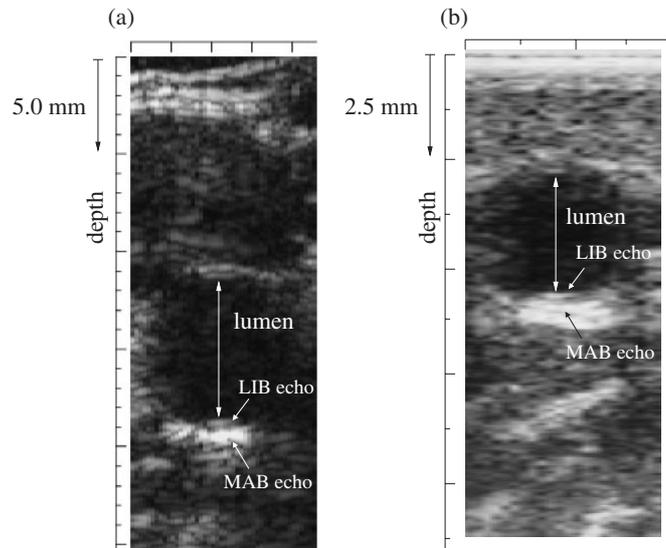
Fig. 1. Reconstructed B-mode images of (a) brachial and (b) radial arteries of 33-year-old male in plane perpendicular to axis of artery.
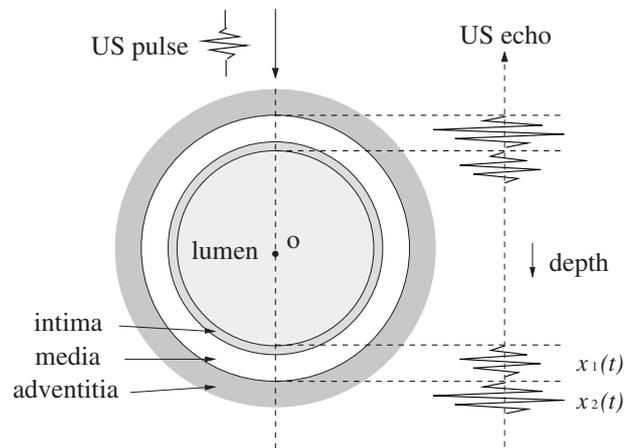
Fig. 2. Schematic view of ultrasonic echo from vessel wall when ultrasonic beam passes through center of artery.

and MAB. Therefore, we modeled the echo from the arterial wall by those from the LIB and MAB, $\hat{x}_1(t)$ and $\hat{x}_2(t)$. The model echoes $\hat{x}_1(t)$ and $\hat{x}_2(t)$ are simulated by referring to the ultrasonic echo from a point scatterer (35-μm-thick fine wire in water), as shown in Fig. 3. The model echoes $\hat{x}_1(t)$ and $\hat{x}_2(t)$ are formulated by multiplying the sinusoidal waves at the center frequencies f_1 and f_2 by the Hanning window $w(t)$, which shows the envelope of an echo, as

$$\hat{x}_1(t) = a_1 \cdot \sin[2\pi f_1(t - \tau_1)] \cdot w_1(t - \tau_1), \qquad (2.4)$$
$$\hat{x}_2(t) = a_2 \cdot \sin[2\pi f_2(t - \tau_2)] \cdot w_2(t - \tau_2), \qquad (2.5)$$
$$w_i(t) = 0.5 - 0.5\cos\left(\frac{2\pi f_i t}{n}\right) \quad (i = 1 \text{ or } 2), \qquad (2.6)$$

where f_1 and f_2 are the center frequencies of the LIB and MAB echoes, a_1 and a_2 are amplitude coefficients of echoes from the LIB and MAB, and τ_1 and τ_2 are time delays of respective echoes, respectively; n is the number of cycles at the center frequency in an echo. As shown in Fig. 3, the model echo is in very good agreement with the measured one. The model echo $\hat{x}(t)$ is expressed by the sum of $\hat{x}_1(t)$ and $\hat{x}_2(t)$ as
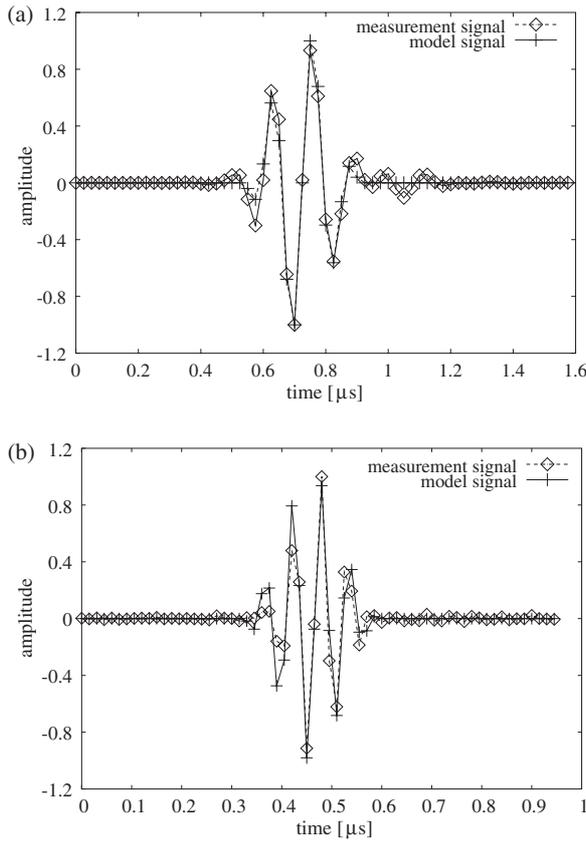
Fig. 3. Measured RF signal [(a) 10 MHz, (b) 22 MHz] from a point scatterer (dashed line) and model signal (solid line).

$$\hat{x}(t) = \hat{x}_1(t) + \hat{x}_2(t). \tag{2.7}$$

The parameters $\{f_i\}$, $\{a_i\}$, and $\{\tau_i\}$ ($i = 1, 2$) are determined such that the difference between the model $\hat{x}(t)$ and measured echo $x(t)$ is minimal. At first, the instantaneous center frequencies $\{f_i\}$ of the measured RF signal are estimated using complex auto-correlation.[17,18] An acquired RF signal is denoted by $x(m)$, where m shows the time mT_s (T_s: sampling period of echoes). The acquired RF signal is quadrature-demodulated by applying

$$\check{x}(m) = \text{LPF}[x(m) \cdot e^{j\omega_{\text{dem}}mT_s}], \tag{2.8}$$

where LPF[·] represents low-pass filtering, and $f_{\text{dem}} = \omega_{\text{dem}}/2\pi$ is the demodulation frequency. To estimate the difference between the demodulation frequency f_{dem} and the actual center frequency f_0, the complex auto-correlation coefficient $R(m')$ at lag $\Delta m = 1$ is calculated as

$$\hat{R}(\Delta m) = \sum_{m=0}^{M-1} \check{x}^*(m) \cdot \check{x}(m + \Delta m), \tag{2.9}$$

where MT_s is set to one wavelength of the ultrasonic signal. From the phase $\angle R(\Delta m)$, the actual RF center frequencies, $\{f_i\}$ ($i = 1, 2$), can be estimated as[18]

$$\hat{f}_i = f_{\text{dem}} - \frac{\angle \hat{R}(\Delta m)}{2\pi T_s} \quad (i = 1, 2). \tag{2.10}$$

The amplitude ratio between the measured RF echo $x(t)$ and the model echo $\hat{x}(t)$, which is composed of $\hat{x}_1(t)$ and $\hat{x}_2(t)$ obtained using the estimated center frequencies $\{f_i\}$, is calculated by the least-squares method. Note that $z(t)$ and

$\hat{z}(t)$ are the complex demodulated signals of $x(t)$ and $\hat{x}(t)$, respectively.

At the preassigned lags τ_1 and τ_2, the normalized mean square error (MSE) α between the measured RF and model echoes is calculated. However, in the case that the MSE is normalized throughout the period to calculate it, the normalized MSE α becomes insensitive to the goodness of fit with respect to $x_1(t)$ because the echo from the LIB is much smaller than that from the MAB. Therefore, the normalized MSE α is separately calculated with respect to the pulse durations of $\hat{x}_1(t)$ and $\hat{x}_2(t)$. The region-to-region normalized MSE α is formulated as

$$\alpha = \frac{\displaystyle\sum_{m \in K \cap \overline{K} \cap L} |z(mT_s) - \hat{z}_1(mT_s)|^2}{\displaystyle\sum_{m \in K \cap \overline{K} \cap L} |z(mT_s)|^2}$$
$$+ \frac{\displaystyle\sum_{m \in L \cap \overline{L} \cap K} |z(mT_s) - \hat{z}_2(mT_s)|^2}{\displaystyle\sum_{m \in L \cap \overline{L} \cap K} |z(mT_s)|^2}$$
$$+ \frac{\displaystyle\sum_{m \in K \cap L} |z(mT_s) - \{\hat{z}_1(mT_s) + \hat{z}_2(mT_s)\}|^2}{\displaystyle\sum_{m \in K \cap L} |z(mT_s)|^2}, \tag{2.11}$$

where $\hat{z}_1(t)$ and $\hat{z}_2(t)$, which correspond to $\hat{x}_1(t)$ and $\hat{x}_2(t)$, are complex demodulated model signals of $\hat{x}_1(t)$ and $\hat{x}_2(t)$ with the pulse lengths K and L, respectively. Figures 4(c) and 4(d) show two cases in which $\hat{x}_1(t)$ and $\hat{x}_2(t)$ overlap and do not overlap, respectively. The overlap of echoes from the LIB and MAB is automatically taken into consideration because the normalized MSE is evaluated between the measured echo $x(t)$ and model $\hat{x}(t)$ which is the sum of $x_1(t)$ and $x_2(t)$. It is shown by the third term on the right-hand side of eq. (2.11) that the difference between the measured $z(t)$ and the sum of the models $\hat{z}_1(t)$ and $\hat{z}_2(t)$ is evaluated. The phase information of the echo from the LIB and that from MAB are considered because $\hat{z}_1(t)$ and $\hat{z}_2(t)$ are complex signals. For the robust detection of the leading edge of an echo from the LIB, a constraint term, β, is added by calculating the variance in $x(t)$ just before the LIB echo, as shown in Fig. 4. The variance β is normalized by the mean power σ^2 in the region of interest before the the model LIB echo $\hat{x}_1(t)$. The magnitudes of echoes from the lumen are so small, and the normalized variance β is nearly zero. On the other hand, β increases when the model LIB echo $\hat{x}_1(t)$ is located on the wall (false detection) because the region shallower than $\hat{x}_1(t)$ is not the lumen in such a situation, and there are echoes. Therefore, the number of cases of false detection can be reduced by adding β. The final form of the normalized MSE γ is given by

$$\gamma = \alpha + \beta, \tag{2.12}$$

$$\beta = \sum_{m=\tau_1/T_s-N}^{\tau_1/T_s} \frac{|x(mT_s)|^2}{\sigma^2}, \tag{2.13}$$

where N is the number of samples necessary for calculating the variance and is set to approximately three wavelengths. According to the above process, the normalized MSE is calculated with respect to each preassigned τ_1 and τ_2. The time delays τ_1 and τ_2 were changed at intervals of $\{\pi/(6\omega_i)\}$
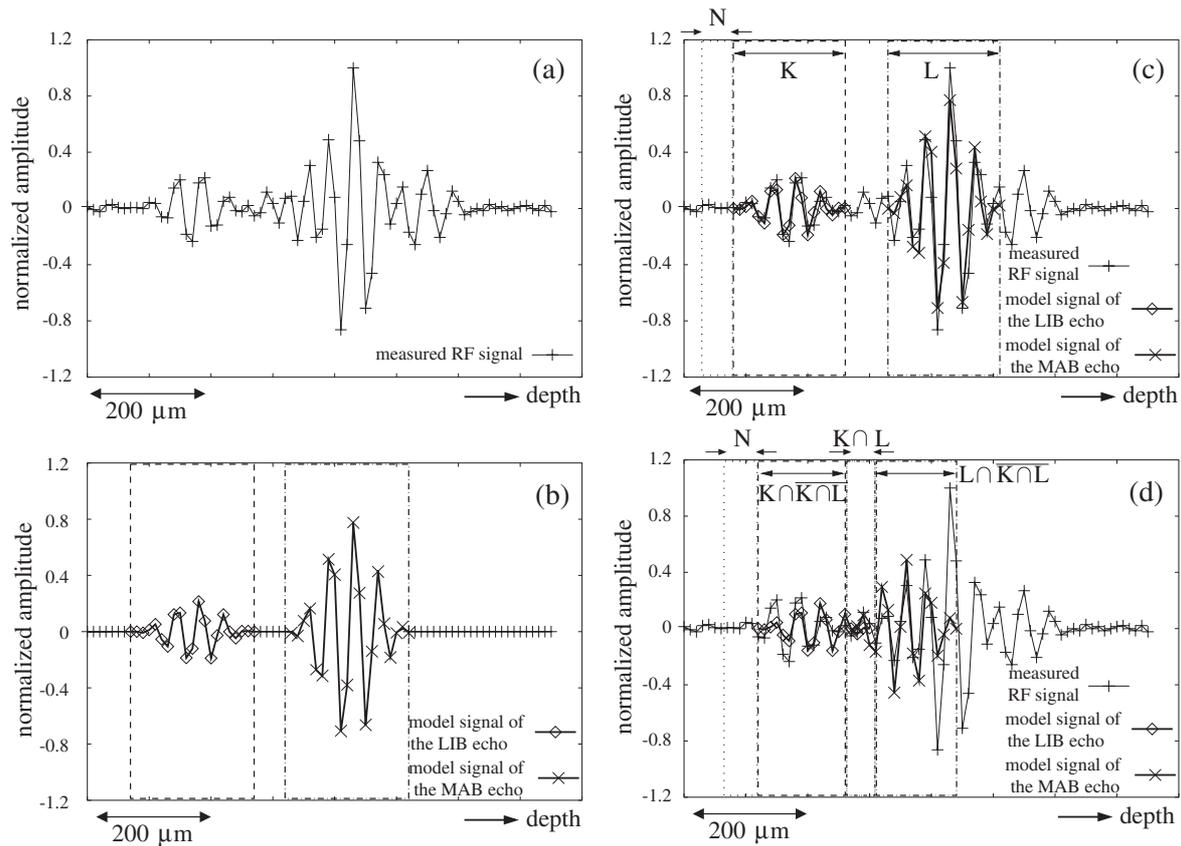
Fig. 4. (a) Measured RF signal. (b) Model signal. Periods for calculating MSE between measured RF signal and model signal in cases of (c) separated $\hat{x}_1(t)$ and $\hat{x}_2(t)$ and (d) overlapped $\hat{x}_1(t)$ and $\hat{x}_2(t)$.

($i = 1, 2$). In this study, the difference $\tau_2 - \tau_1$ ranged from 100 to 500 μm by referring to the typical intima-media thickness.[19,20] The time delays τ_1 and τ_2 that minimize the normalized MSE between the measured RF signal and model signal are determined as the optimum boundary positions k and l, respectively.

2.3 In vivo measurement

In this study, the right brachial and radial arteries of a healthy subject (subject A: 33-year-old male) and the right brachial arteries of three healthy subjects (subjects B, C, D: 22-year-old males) are measured. In the measurement of the brachial artery, the RF echoes were acquired using a 10 MHz linear-type ultrasonic probe of ultrasonic diagnostic equipment (SSD-6500, Aloka). The received echoes are acquired at a sampling frequency of 40 MHz. At first, we measured the electrocardiogram and RF echoes during two consecutive heartbeats for 2 min at intervals of about 20 s at rest. Then, blood flow is stanched by surrounding the forearm with a cuff at a pressure of 250 mmHg for 5 min. After the release of the cuff, NO, which is generated by the endothelium in response to the shear stress due to increased blood flow, makes the smooth muscle in the media to relax. RF echoes are acquired for 3 min at an interval of about 12 s after the release of the cuff. For the measurement of the same position where the intima-media region of the brachial posterior wall is clearly imaged, the ultrasonic probe was held by the pointsetter. Blood pressure was continuously measured at the wrist with a spygnomanometer, and the

systolic and diastolic blood pressure in each measurement were recorded.

For the measurement of the radial artery, sets of RF echoes were acquired using a 22-MHz linear-type ultrasonic probe of another modified ultrasonic diagnostic equipment (Diasus, Dynamic Imaging). The received echoes are acquired at a sampling frequency of 66.5 MHz using a custom-made system. The measurement procedure is similar to that for the brachial artery described above.

3. In vivo Experimental Results

3.1 Example of complex template matching

Figure 5 shows the results of applying the complex template matching method to a measured RF echo. Figures 5(a) and 5(b) show the normalized MSE distributions $20 \log_{10} \alpha$ and $20 \log_{10} \gamma$ without and with a constraint term, respectively. As shown in Fig. 5(a), the MSE without β converges at several combinations of τ_1 and τ_2. In contrast, MSE converges at one point in accordance with the constraint, as shown in Fig. 5(b).

The RF signals and envelopes of the measured signal and the echo model at point A in Fig. 5(a) are shown in Fig. 6. The estimated frequencies of the LIB and MAB echo models are respectively 17.57 and 17.17 MHz, and the echo models are in good agreement with the measured signal. The model can represent the measured signal very well because the MSE α at point A in Fig. 5(a) is 12%.

Figure 7 shows the result of the boundary detection for the several ultrasonic beams in a B-mode image along the

(a)

(b)
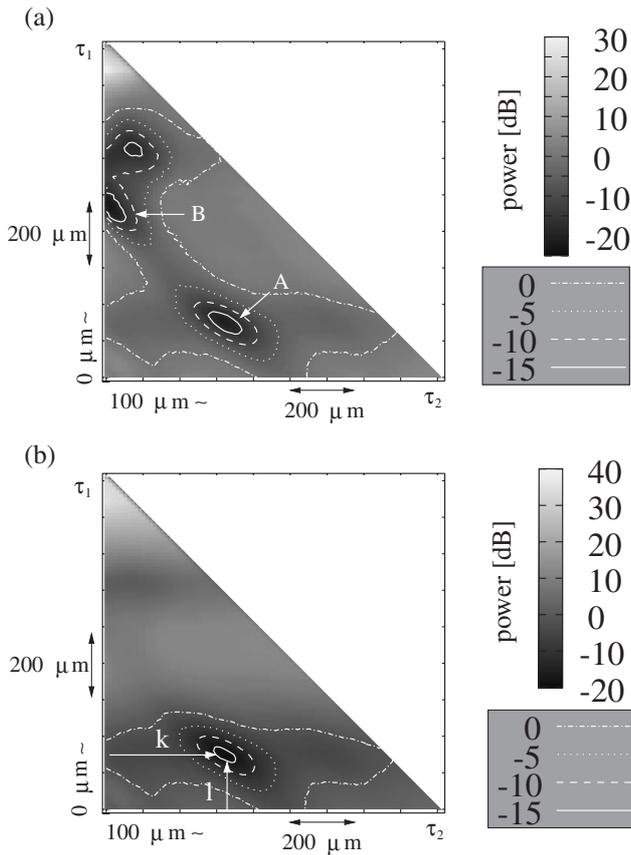
Fig. 5.   Results of applying complex template matching to RF data. (a) $20 \log_{10} \alpha$ vs time delays τ_1 and τ_2. (b) $20 \log_{10} \gamma$ vs time delays τ_1 and τ_2.
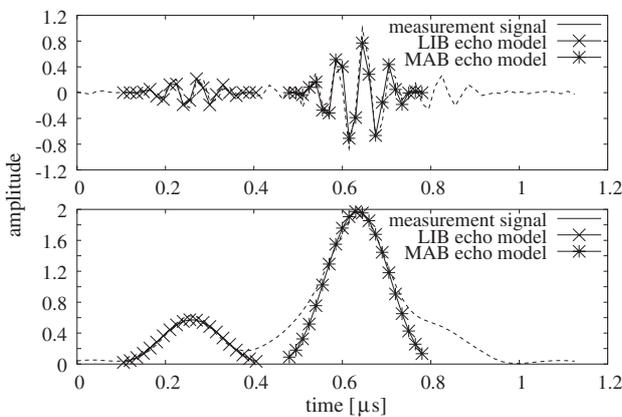
Fig. 6.   RF signal and envelope of measured signal and echo models.

longitudinal direction of the radial artery. As shown in Fig. 7, the boundary positions, which are shown as k and l on the B-mode image, are detected appropriately and objectively by complex template matching.

3.2   Measurement in brachial artery

Figure 8 shows an example of measurement of the change in intima-media thickness in the healthy 33-year-old male during two consecutive heartbeats for 3 s at rest. As shown in Fig. 8(a), the initial positions k and l of the lumen-intima and media-adventitia boundaries of the brachial artery on the M-mode image were determined by the method described in

(a)   (b)
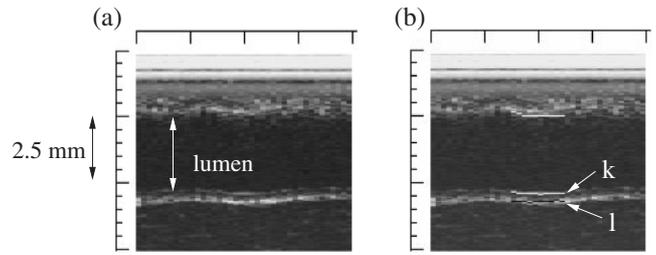
Fig. 7.   (a) Reconstructed B-mode image in long-axis view of radial artery of 33-year-old male. (b) Result of boundary detection using complex template matching.
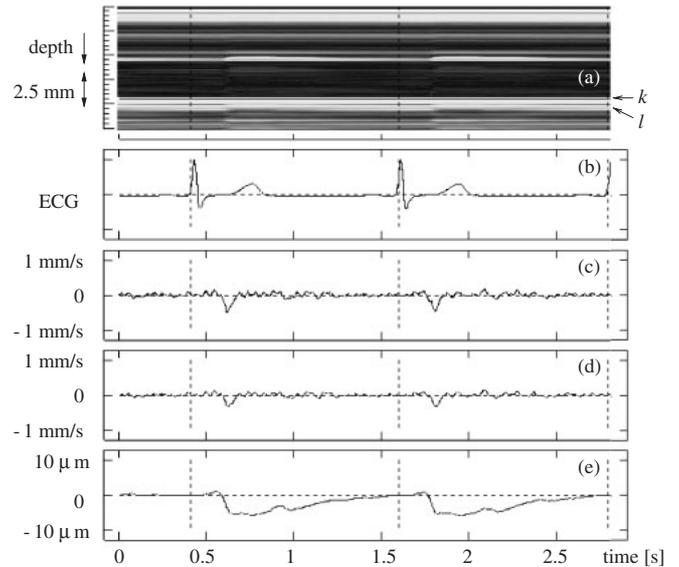
Fig. 8.   (a) M-mode image of brachial artery (healthy 33-year-old male). (b) Electrocardiogram. (c) Velocity at point k assigned as LIB. (d) Velocity at point l assigned as MAB. (e) Change in intima-media thickness.

§2.2, and then the instantaneous positions of these points were automatically tracked as shown by black lines using the *phased tracking method*. Figures 8(c) and 8(d) show the estimated velocities at k and l, respectively. The change in the thickness of the intima-media complex was calculated by the temporal integration of the difference between these velocities, as shown in Fig. 8(e). The elastic modulus of the intima-media region of the brachial artery for each measurement was calculated using the estimated maximum change in thickness and the pulse pressure, as described in §2.1.

Figure 9 shows the transients in the maximum change in the thickness of the intima-media region of the brachial arterial wall during one cardiac cycle and the pulse pressure in each measurement. The change in thickness and the pulse pressure at each RF acquisition during 10 min are plotted by crosses and diamonds, respectively. About 20 to 40 s after the release of the cuff, the change in thickness increased compared with that at rest, as shown by the dashed line in Fig. 9. Then, the change in thickness gradually returned to that at the rest.

Figure 10 shows the transients in the change in inner diameter manually obtained from the B-mode image at each R-wave of the electrocardiogram and the change in elasticity, which is calculated by the maximum change in
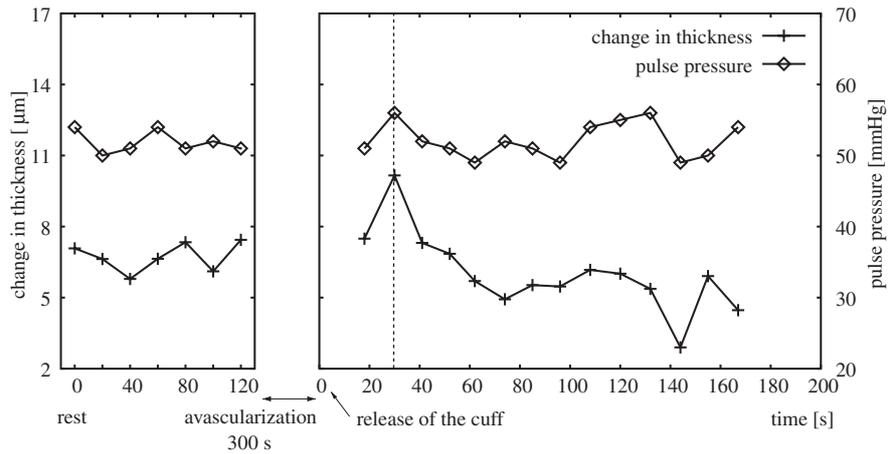
Fig. 9.   Transient changes in maximum change in thickness of intima-media region of brachial artery and pulse pressure (healthy 33-year-old male).
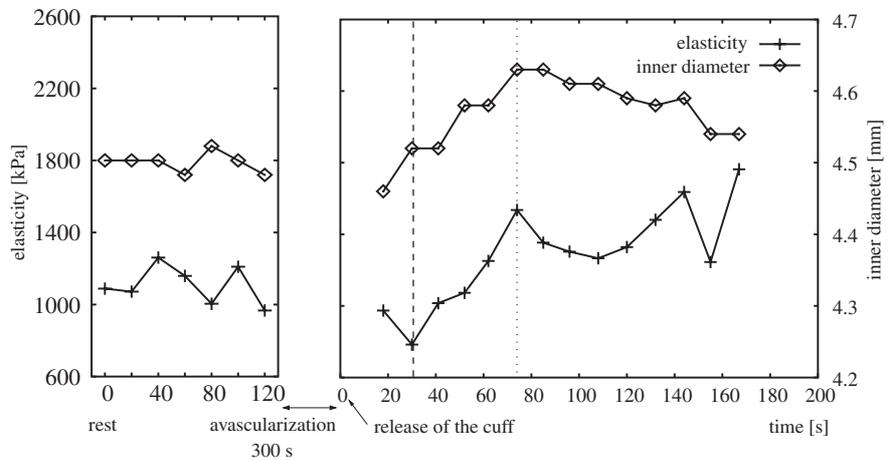
Fig. 10.   Transient changes in elasticity of intima-media region of brachial artery and inner diameter (healthy 33-year-old male).

the thickness of the intima-media region in each measurement. The inner diameter and change in elasticity at each RF acquisition over 10 min are plotted by diamonds and crosses, respectively. From about 20 to 40 s, the maximum decrease in elasticity shown by the dashed line compared with the averaged elasticity at rest was 29.3%. The inner diameter shown by the dotted line increased by 3.0% compared with the averaged inner diameter at rest about 70 s after the release of the cuff. These results are comparable with those previously measured for the brachial artery.[8,13,15]

3.3   Measurement of radial artery

Figure 11(a) shows an M-mode image of the radial artery of the same subject shown in Fig. 8. Figures 11(c) and 11(d) show the estimated velocities at points k and l, respectively. The change in the thickness of the intima-media complex was calculated by temporal integration of the difference between these velocities, as shown in Fig. 11(e). The subcutaneous tissue on the radial artery is less than that on the brachial artery as shown in Fig. 1.

Figure 12 shows the maximum change in thickness of the intima-media region of the radial artery estimated at five neighboring ultrasonic beams during one cardiac cycle and the pulse pressure in each measurement. The averages of the
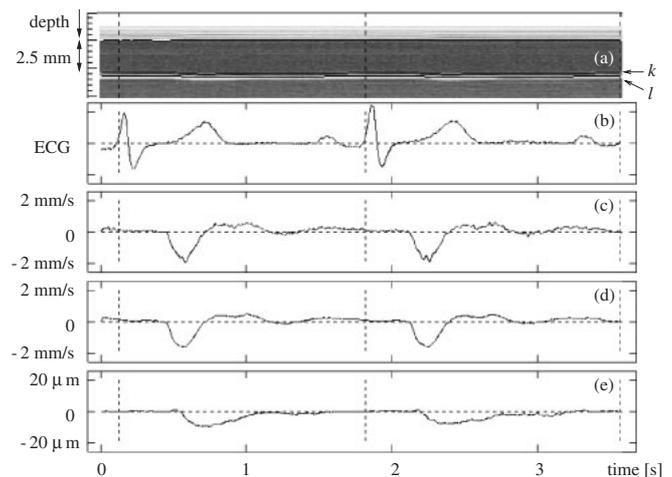
Fig. 11.   (a) M-mode image of radial artery (healthy 33-year-old male). (b) Electrocardiogram. (c) Velocity at point k assigned as LIB. (d) Velocity at point l assigned as MAB. (e) Change in intima-media thickness.

maximum changes in the intima-media thickness in five contiguous beams are plotted by crosses, and the vertical bars show the standard deviations. About 40 to 60 s after the release of the cuff, the maximum change in the thickness
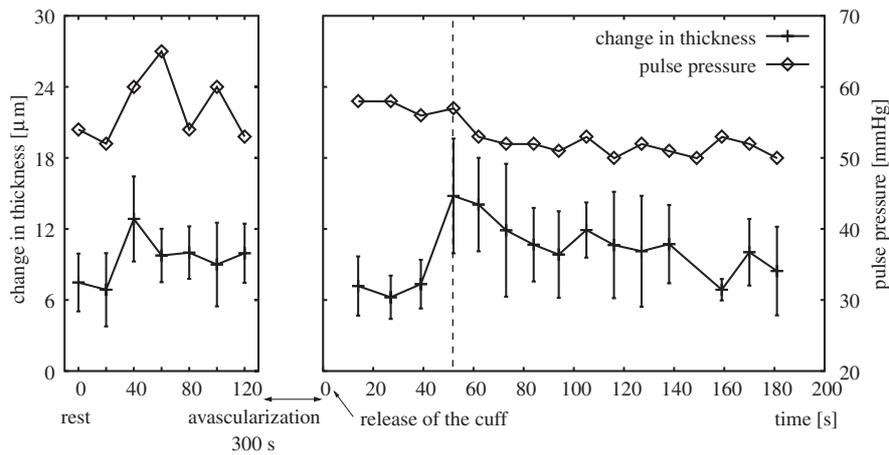
Fig. 12.   Transient changes in maximum change in thickness of intima-media region of radial artery and pulse pressure (healthy 33-year-old male).
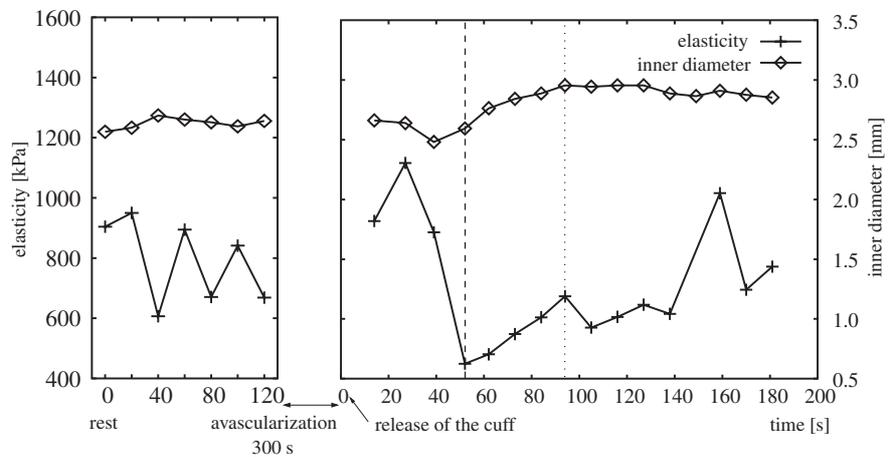
Fig. 13.   Transient changes in elasticity of intima-media region of radial artery and inner diameter (healthy 33-year-old male).

becomes maximum as well the measurement for the brachial artery.

Figure 13 shows the transients in inner diameter and elasticity, which is calculated from the average of the maximum changes in thickness at five beams in each measurement. About 40 to 70 s after the release of the cuff, the maximum decrease in elasticity compared with the averaged elasticity at rest was 43.0%. The maximum increase in inner diameter was 10.1% compared with the averaged inner diameter at rest about 90 s after the release of the cuff. These results are comparable with those measured for the brachial artery shown in Figs. 9 and 10.

3.4 Relationship between maximum increase in inner diameter and maximum decrease in elasticity

The brachial arteries of subjects B, C, and D as well as that of subject A are measured. The relationship between the maximum increase in inner diameter and the maximum decrease in elasticity for each subject is shown in Fig. 14. As shown in Fig. 14, a negative correlation between the maximum increase in inner diameter and the maximum decrease in elasticity is confirmed; it was found that the rate of change obtained by the proposed method is much larger than that obtained by the conventional method. Moreover,
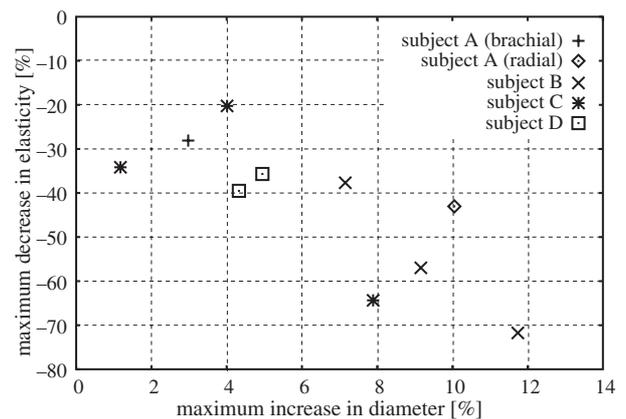
Fig. 14.   Relationship between maximum increase in inner diameter and maximum decrease in elasticity for each subject.

the rate of change in the measurement of the radial artery is much larger than that of the brachial artery as shown by the results of subject A.

4. Discussion

In §3.4, the results of the measurement of the endothelium-dependent relaxation response of the brachial and
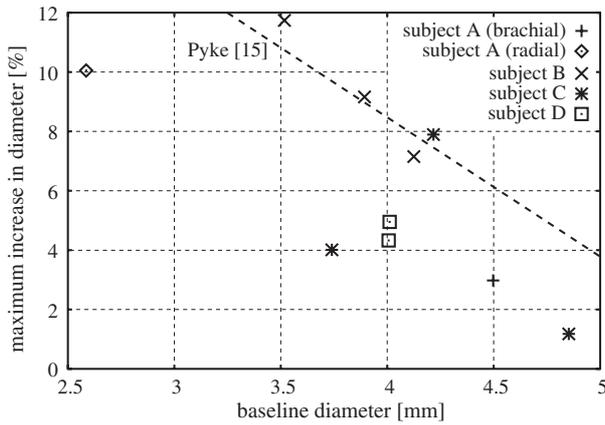
Fig. 15. Relationship between inner diameter at rest and maximum increase in inner diameter.

radial arteries are shown. As shown in Fig. 14, compared with that for the brachial artery, the % maximum increase in inner diameter and % decrease in the elasticity of the radial artery were large. On the other hand, the rates of change in the measurement of the identical subject had a characteristic variation. Thus, we tried to explain the cause of the above result.

The arterial wall consists of elastic fibers, collagenous fibers and smooth muscle. The contents, sequences, and distribution of these components differ depending on the type of artery and age.[21] In particular, elastic arteries such as the aorta are rich in elastic fibers, and muscular arteries such as the brachial and radial arteries, are rich in smooth muscle, which actively extends the artery to adjust blood flow. In systemic circulation, the amount of elastic fibers and smooth muscle increases from the aorta to the peripheral vessel.[22] Therefore, it is considered that the rate of FMD of the radial artery is much larger than that of the brachial artery because the radial artery, which is more peripheral, is rich in smooth muscle cells responding to NO.

Another reason is the difference in the magnitude of the shear stress exerted on the arterial wall due to blood flow. Shear stress exerted on the radial arterial wall is larger due to the smaller diameter of the artery because a smaller vascular diameter significantly increases flow rate.[15] The relationship between the inner diameter at rest and the maximum change in the inner diameter of each subject is shown in Fig. 15. As shown in Fig. 15, the characteristics of the rates of change in the measurement of the brachial artery agree with those provided by Pyke *et al.*[15] Therefore, it is important to measure the FMDs in the arteries with similar diameters to compare different subjects.

5. Conclusions

In this study, we significantly reduced the ambiguity in assigning the lumen-intima and media-adventitia boundaries using complex template matching. The transient change in elasticity only for the intima-media region of the brachial

and radial arteries due to endothelium-dependent flow-mediated dilation was measured. The normalized change in elasticity measured by the proposed method was much larger than the normalized change in diameter measured by conventional methods, which evaluate the mechanical property of the entire wall. Moreover, it is supposed that the change in the inner diameter and the elasticity of the radial artery are larger than those of the brachial artery because the radial artery is rich in smooth muscle cells which respond to NO, and the magnitude of the shear stress to the arterial wall is also larger. From these results, we demonstrated the possibility of the sensitive assessment of endothelial dysfunction at the radial artery using high-accuracy boundary detection.

1) R. Ross: New Engl. J. Med. **340** (1999) 115.
2) T. Reichlin, A. Widl, M. Dürrenberger, A. U. Daniels, U. Aebi, P. R. Hunziker, and M. Stolz: J. Struct. Biol. **152** (2005) 52.
3) P. C. G. Simons, A. Algra, M. L. Bots, D. E. Grobbee, and Y. van der Graaf: Circulation **100** (1999) 951.
4) T. Mashiyama, H. Hasegawa, and H. Kanai: Jpn. J. Appl. Phys. **45** (2006) 4722.
5) H. Kanai, H. Hasegawa, and N. Nakagawa: *State of the Art: Ultrasonics in Medicine* (Elsevier, Amsterdam, 2004) International Congress Series, Vol. 1274, p. 64.
6) J. Inagaki, H. Hasegwa, and H. Kanai: Jpn. J. Appl. Phys. **45** (2006) 4732.
7) H. Kanai, H. Hasegawa, F. Tezuka, and Y. Koiwa: Circulation **107** (2003) 3018.
8) M. C. Corretti, T. J. Anderson, E. J. Benfamin, D. Celermajer, F. Charbonneau, M. A. Creager, J. Deanfield, H. Drexler, M. Gehard-Herman, D. Herrington, P. Vallance, J. Vita, and R. Vogel: J. Am. College Cardiol. **39** (2002) 257.
9) L. Fan, P. Santago, H. Jiang, and D. M. Herrington: IEEE Trans. Med. Imaging **19** (2000) 621.
10) G. M. Buga, M. E. Gold, J. M. Fukuto, and L. J. Ignarro: Hypertension **17** (1991) 187.
11) H. Kanai, M. Sato, Y. Koiwa, and N. Chubachi: IEEE Trans. Ultrason. Ferroelectr. Freq. Control **43** (1996) 791.
12) H. Hasegawa, H. Kanai, N. Hoshimiya, and Y. Koiwa: J. Med. Ultrason. **31** (2004) 81.
13) M. Sugimoto, H. Hasegwa, and H. Kanai: Jpn. J. Appl. Phys. **44** (2005) 6297.
14) L. Fan, P. Santago, W. Riley, and D. M. Herrington: Ultrasound Med. Biol. **27** (2001) 399.
15) K. E. Pyke and M. E. Tschakovsky: J. Physiol. **568** (2005) 357.
16) A. D. M. Swijndregt, S. H. K. The, E. J. Gussenhoven, C. T. Lanée, H. Rijsterborgh, E. Groot, A. F. W. Steen, N. Bom, and R. G. A. Ackerstaff: Ultrasound Med. Biol. **22** (1996) 1007.
17) X. Lai, H. Torp, and K. Kristoffersen: IEEE Trans. Ultrason. Ferroelectr. Freq. Control **44** (1997) 1332.
18) S. I. Rabben, S. Bjærum, V. Sørhus, and H. Torp: Ultrasound Med. Biol. **28** (2002) 507.
19) T. Furumoto, S. Fujii, K. Nishihara, S. Yamada, K. Komuro, K. Goto, H. Onozuka, T. Mikami, A. Kitabatake, and B. E. Sobel: Am. J. Cardiol. **93** (2004) 997.
20) D. P. Germain, P. Boutouyrie, B. Laloux, and S. Laurent: Arterioscler. Thromb. Vasc. Biol. **23** (2003) 836.
21) K. Hayashi, S. Nagasawa, Y. Naruo, A. Okumura, K. Moritake, and H. Handa: Biorheology **17** (1980) 211.
22) J. T. Apter, M. Rabinowitz, and D. H. Cummings: Circ. Res. **19** (1966) 104.